Synchrotron x-ray transmission measurements and modeling of filters investigated for Athena

Elena Puccio,[a,b,*] Michela Todaro,[a,b] Ugo Lo Cicero,[a,b] Luisa Sciortino,[a,b] Philippe Laurent,[c] Philippe Ferrando,[c] Angelo Giglia,[d] Stefano Nannarone,[d] and Marco Barbera[a,b]

[a]Università degli Studi di Palermo, Dipartimento di Fisica e Chimica—Emilio Segrè, Palermo, Italy

[b]Italian National Institute for Astrophysics, Osservatorio Astronomico di Palermo Giuseppe S. Vaiana, Palermo, Italy

[c]Université Paris-Saclay, Université Paris, Astrophysique Instrumentation Modélisation, Centre for Extragalactic Astronomy, Centre National de la Recherche Scientifique, Gif-Sur-Yvette, France

[d]Consiglio Nazionale delle Ricerche-Istituto Officina dei Materiali, Trieste, Italy

Abstract. Advanced Telescope for High-Energy Astrophysics is a large-class astrophysics space mission selected by the European Space Agency to study the theme "Hot and Energetic Universe." The mission essentially consists of a large effective area x-ray telescope and two detectors: the X-ray Integral Field Unit (X-IFU) and the Wide Field Imager (WFI). Both instruments require filters to shield from out-of-band radiation while providing high transparency to x-rays. The mission is presently in phase B; thus, to consolidate the preliminary design, investigated filter materials need to be properly characterized by experimental test campaigns. We report results from high-resolution x-ray transmission measurements performed using different synchrotron radiation beamlines to assess the filter calibration accuracy and mitigate the risk related to selecting a unique calibration facility. The main goals of these test campaigns are (i) to verify the compliance of the investigated filter design to the scientific requirements, (ii) to develop an accurate x-ray transmission model, and (iii) to start identifying suitable measurement facilities and achievable accuracy for the flight filters calibration program. In particular, the x-ray transmission model of the X-IFU and WFI filters has been refined within the edges of Al, C, N, and O by deriving the optical constants from two reference samples measured by synchrotron light. The achievable filter calibration accuracy has been estimated by evaluating the agreement between the best-fit according to the developed transmission model and the experimental data. [DOI: 10.1117/1.JATIS.6.3.038003]

Keywords: x-ray transmission; astrophysics space mission Athena; X-ray Integral Field Unit; Wide Field Imager; optical and thermal filters.

Paper 20044 received May 6, 2020; accepted for publication Aug. 13, 2020; published online Sep. 4, 2020.

1 Introduction

In the Cosmic Vision 2015 to 2025 Science program of the European Space Agency (ESA), Advanced Telescope for High-Energy Astrophysics (Athena) has been selected as a large-class astrophysics mission to study the dynamical, physical, and chemical properties of hot plasma in the Universe and to understand the role of black holes in shaping the environment, from local accretion disks to galaxy cluster scales.[1] The mission, with the launch scheduled in 2033, is presently in phase B, which ends with the Mission Adoption Review by the ESA at the end of 2021.

Athena will be equipped with a large effective area (~1.5 m^2 at 1 keV) grazing incidence x-ray telescope with a focal length of 12 m and two interchangeable focal plane detectors:

*Address all correspondence to Elena Puccio, E-mail: elena.puccio@inaf.it

2329-4124/2020/$28.00

Table 1 X-IFU QE and filter transmission requirements for the comprehensive filter stack.

Energy (keV)	X-IFU QE (%)	T_{filters} (%)
0.35	≥17	≥21
1	≥67	≥76
7	72	≥89
9.5	≥50	≥89

the X-ray Integral Field Unit (X-IFU),[2] a microcalorimeter made of a hexagonal array of molybdenum-gold transition-edge sensors,[3] and the Wide Field Imager (WFI),[4] a large array of depleted field-effect transistors (DEPFET) active pixels. The X-IFU is a cryogenic x-ray spectrometer operating at a temperature of about 50 mK from 0.2 to 12 keV energy range to offer high spectral resolution (2.5 eV FWHM at 7 keV) over a field of view of a 5–arc min equivalent diameter. The WFI instrument is based on an array of silicon detectors covering a field of view of 40×40 arc min^2 with a small detector of the same type, featuring high count rate capability, to observe very bright point sources in the 0.2 to 15 keV energy range over a wide field.

Both instruments require filters to attenuate out-of-band radiation, which is similar to optical and thermal filters already used for other instruments, such as the high resolution camera[5] and Advanced CCD Imaging Spectrometer (ACIS)[6] detectors on Chandra[7] and the Soft X-Ray Spectrometer (SXS) microcalorimeter on ASTRO-H (Hitomi).[8,9] Indeed, the X-IFU detector must be shielded from incoming ultraviolet–visible–infrared (UV–Vis–IR) radiation due to both the optical load from bright UV–Vis astrophysical sources (e.g., massive stars and active galactic nuclei) and the infrared (IR) radiation heat load from the instrument, which would degrade its energy resolution due to photon shot noise.[10–12] The X-IFU filters are each to be mounted on one of five thermal shields at the operating temperatures of 300, 100, 30, 2, and 0.05 K, thus becoming an integral part of the thermal engineering of the cryostat. Likewise, the DEPFET active pixel sensors of the WFI[13] are sensitive to UV–Vis photons with energies above the Si bandgap (∼1.1 eV).

The comprehensive filter stack in the X-IFU instrument should allow for an x-ray transmission compliant with the quantum efficiency (QE) requirements[14] given in Table 1. Transmission requirements[15] are derived from the QE for the whole X-IFU instrument, which is given by the product of the filter stack transmission and the detector QE. Since the X-IFU QE at low energy mostly depends on filter transmission, a filter must be extremely thin, while still compliant with both out-of-band radiation attenuation and mechanical requirements.

Before launch, both onboard instruments must be calibrated. The resolution of X-IFU is expected to be ∼2.5-eV FWHM; thus, during calibration, the photoelectric absorption edge structure should be resolved by a factor ∼10 better than the resolution required, with an absolute energy knowledge better than 0.4 eV. The calibration accuracy on the total X-IFU QE (filters and detector), currently identified in the calibration plan,[16] is the lowest between 4% absolute (0.04) in a given energy bin and 3% relative to the transmission in that bin, over the full-energy range of interest, or a fixed value of 0.01 when QE is <0.33. Calibration accuracy within edges is required to be 3% on ground. However, the allocation budget on calibration accuracy between the subsystems, namely, filters and detector, is yet to be defined, and it is assumed to be mostly allocated to the filter full stack at lower energies, where their QE is lowest and the detector one is highest, whereas the opposite is true on the higher end of the energy range. Calibration of single filters can be performed, and the requirement is met by the square sum of all filter calibration accuracies.

Given such demanding calibration requirements, we have started, as part of the research activities for the design and development of Athena X-IFU thermal filters and WFI optical filters, a campaign of x-ray transmission measurements on a set of representative filter samples made of a thin layer of polyimide (PI) coated with aluminum (Al), using different synchrotron radiation facilities. Filter materials are chosen with a low atomic number Z, to have a high transmission in the energy band of interest while shielding the IR and near-infrared (NIR) energy ranges (PI), whereas the Al coating has the ulterior purpose of reflecting the UV/Vis part of the spectrum. Prior work was carried out on the calibration of aluminized PI films to be used as filters for

previous x-ray astronomy missions.[17–19] The main goals of this campaign are to verify the compliance of the baseline filter design to the scientific requirements, to develop an accurate x-ray transmission model for the filters, especially within element absorption edges, and to start identifying suitable measurement facilities.

2 Materials and Methods

2.1 *Measured Samples*

Samples, produced by LUXEL (USA), are made of a PI ($C_{22}H_{10}N_2O_4$) layer of either ~45 or ~150 nm, coated with a thin Al layer of either ~20 or ~30 nm. Samples with a thin PI layer are representative of the baseline for thermal filters inside the detector cooling system for the X-IFU instrument, whereas those with a thick PI layer are investigated as the baseline for the optical blocking filter of the WFI instrument.

Henceforth, all samples will be denoted by the following label: Al thickness/PI thickness in nanometers (e.g., 20/45 or 30/150). Filters are baselined to be further equipped with a honeycomb Au/Ag-plated stainless steel (SS) or Nb mesh with a 5-mm pitch between cells, cell bars 50 to 90 μm wide, and a total blocking factor of about 2% [see Fig. 1(a) for a filter prototype]. The mesh serves multiple purposes, such as structural strength, vibrational rigidity, and improved thermal conductivity. However, for ease of measurement, the samples used in these campaigns are smaller, meshless versions mounted on a TF111/TF110 standard LUXEL frame [see Fig. 1(b)].

This choice is due to the fact that, in terms of x-ray transmission, the meshless samples can be thought of as a single cell of the full-scale filter since the beam spot never exceeds a diameter of 1.2 mm and is entirely contained in a 5-mm mesh cell. Design is still ongoing on mesh materials and geometrical properties. Nominal layer thicknesses and manufacturing tolerances are given in Table 2. Only two samples come from the same production batch, and measurements could not

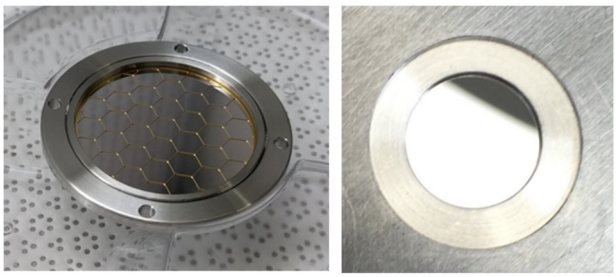

(a) (b)

Fig. 1 Sample filters with a thin PI membrane, coated with Al. (a) Filter sample with a 5-mm pitch Au-plated SS honeycomb mesh mounted on a TF130 standard frame. (b) Meshless filter sample mounted on a TF110 standard frame, as used in the campaigns here reported.

Table 2 Nominal layer thicknesses of Al and PI for each sample with its tolerances from the manufacturer displayed in parenthesis. Next to each sample, in parenthesis, is indicated the synchrotron facility where it was measured.

Sample (synchrotron)	PN	Al (nm)	PI (nm)
20/45 (Elettra)	3203	20.6 (2.5)	45.5 (5)
20/45 (SOLEIL)	3204	20.6 (2.5)	45.5 (5)
20/45 (BESSY II)	2472	21.5 (2.5)	42.7 (5)
30/150 (Elettra)	3096	31.1 (5)	149.7 (5)
30/150 (SOLEIL)	2677	28.8 (5)	153.4 (5)
30/150 (BESSY II)	2460	30.4 (5)	157.8 (5)

be repeated on the same sample in different facilities since samples underwent several types of tests, some of which are destructive, whereas synchrotron measurements span over three years.

2.2 *Synchrotron Facilities*

Three synchrotron facilities were selected to measure the EUV-soft x-ray transmission of samples.

1. CNR-IOM BEAR beamline at Elettra (Trieste, Italy), for its capability of performing measurements at the C K-edge[20]
2. PTB-EUV beamline at BESSY II (Berlin, Germany), for its wide energy range including the Al K-edge.[21]
3. METROLOGIE beamline at SOLEIL (University of Paris-Saclay, France), also for its wide energy range.[22]

The energy ranges investigated include edges of Al, C, N, and O, the elements present in each filter representative sample (see Table 3).

An edge region usually spans from ~10 eV before the edge (pre-edge) to ~50 to 100 eV after it (postedge). Edge regions have to be included in the QE requirements evaluation in calibration tests. Beamline measurement conditions adopted in each campaign are given in Table 4.

2.2.1 *Transmission measurement*

The experimental procedure to obtain each filter transmission is described with reference to the BEAR beamline.[23] At the end of this section, relevant differences between beamline specific procedures are outlined.

Table 3 Atomic L- and K-edges indicative energy ranges in the measured samples.

Element	L-edges (eV)	K-edge (eV)
Al	73 and 118	1560
C	—	284
N	—	402
O	—	532

Table 4 Measurement parameters adopted for the campaigns at BEAR (Elettra in Trieste, Italy), PTB-EUV (BESSY II in Berlin, Germany), and METROLOGIE (SOLEIL in Paris, France) beamlines.

	BEAR at Elettra	PTB-EUV at BESSY II	METROLOGIE at SOLEIL
Spot size	0.4×0.7 mm^2 ($V \times H$)	1.2×1 mm^2 ($V \times H$)	0.6 to 1×1 mm^2 ($V \times H$)
Spectral resolution	$E/\Delta E \sim 2000$	$E/\Delta E > 1000$	$E/\Delta E > 1000$
Energy range	40 to 1650 eV	55 to 1800 eV	30 to 2000 eV
Energy step	0.05 eV	2 to 20 eV outside edge regions	1 to 2 eV outside edge regions
		0.2 to 0.4 eV inside edge regions	0.2 to 0.5 eV inside edge regions
Number of data points	~32,000	~800	~3000

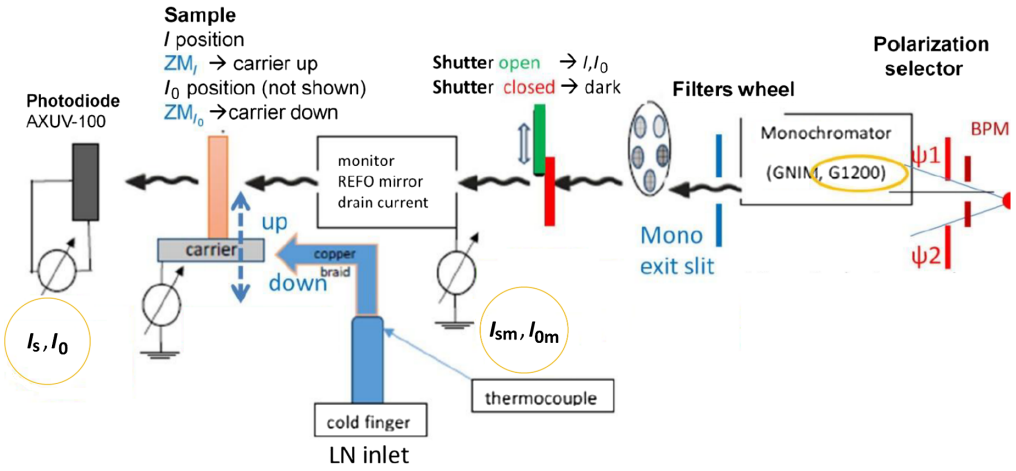

Fig. 2 Conceptual scheme of the BEAR beamline, downstream from synchrotron (Elettra) on the right (not shown): BPM, polarization selector (not used, fully open in these runs), PMPG monochromator, exit slit and filter wheel, light shutter, refocusing mirror (REFO) refocusing mirror, sample stage (cooling system not used in these runs) with sample mounted and beam in/out movements in the experimental chamber (base pressure low 10^{-9} mbar) together with light detector (Absolute X-Ray photodiode series AXUV-100 diode). Instruments indicate p-Ammeters measuring monitor current, sample drain current (not used in these runs), and diode current. BPM plates drain current p-Ammeters not shown in figure.

The conceptual scheme of BEAR is shown in Fig. 2. The monochromator beamline is based on an entrance slitless paraboloidal mirror plane grating (PMPG) [24] optical layout, where the paraboloidal mirror collimates the radiation beam on a couple of plane optical elements, a mirror and a grating, followed by a second paraboloidal mirror, focusing the beam on the exit slit. The inclusion angle was continuously changed along the scan according to a preset working curve to mitigate the higher orders contributions. In addition, a suite of high-energy cutoff filters were used, including an Al filter 0.2-μm thick in the range 40 to 72 eV, a Si filter 0.5-μm thick in the range 72 to 100 eV, and two Ag filters, one 0.6-μm thick in the range 250 to 320 eV and the other 1-μm thick in the range 1100 to 1600 eV.

The photon beam intensity $\Phi(\hbar\omega)$, both impinging and transmitted, were measured by an AXUV-100 photodiode. The reduction of incident photons per second was accomplished as

$$\Phi(\hbar\omega) = I(\hbar\omega)/[e \cdot f(\hbar\omega)], \tag{1}$$

where $I(\hbar\omega)$ is the picoammeter current (I_S and I_0 for transmitted and impinging photon beam, respectively), e is the electron charge, and $f(\hbar\omega)$ is the diode QE.

The I_S and I_0 currents were measured in two separate runs (acquisition times t_1 and t_2). The I_0 signal was acquired removing the sample (sample in/out in Fig. 2) from the measuring position.

The transmission (T) was obtained as

$$T(\hbar\omega) = \frac{I_S(\mathrm{t1}) - I_{Sd}(\mathrm{t3})}{I_{Sm}\,(t1) - I_{Smd}(t3)} \cdot \frac{I_{0m}(\mathrm{t2}) - I_{0md}(t4)}{I_0(\mathrm{t2}) - I_{0d}(t4)}, \tag{2}$$

where the currents with the m subscript indicate the simultaneous monitor signals of the transmitted/impinging beam, that is, the emission current of the refocusing mirror (REFO in Fig. 2) or beam position monitoring (BPM) drain current (see Fig. 2) used in the regions of low impinging intensity (typically the C K-edge). Monitor signals allow for normalization of I_S and I_0, taking into account any impinging flux variation with time, mainly due to synchrotron beam decay (Elettra works in top-up mode, typically percent over hours), together with any beam fluctuation due to beam steering.

The d subscripts in Eq. (2) indicate dark currents from reading picoammeters. The consequent correction is crucial at the low-intensity regions, especially in the C K-edge region,

where optics reflection is reduced by carbon contamination of optical surfaces. A schematic of the BEAR beamline setup is shown in Fig. 2.

A similar procedural scheme was adopted at Metrologie and PTB-EUV, with their particular instrumentation solutions and setups.[25–27] The light spot at the sample and energy step for all beamlines are given in Table 4. The C K-edge was not acquired at PTB-EUV, and I_0 signal was recorded before and after each Is signal and averaged out, whereas at Metrologie no correction for dark current was implemented, a fact that negatively affects the signal-to-noise ratio in low-intensity regions such as the C K-edge.

3 Quantitative Modeling of Filter Transmission

A numerical modeling of a filter transmission, together with a method for recovering optical cross sections from experimental data, is presented. The model achievable accuracy in predicting filter transmission over the energy range of interest is assessed, which is important for planning the calibration activity of the flight filters.

A filter is a multilayer of thin films, differing in thickness, atomic species, and relative concentration, and its transmission curve can be divided into two regions: outside and inside edges. Reliable literature values of the optical constants can be found for outside edge regions;[28] however, this is not the case for inside edge regions. Thus, the optical constants within edges were obtained from experimental data, after fitting outside element edges using a model of the filter transmission. The filter is described as a stack of thin films made of three materials: Al, PI, and aluminum oxide. A layer of native aluminum oxide is introduced, since its presence is known from the literature,[29–31] with a stoichiometry Al_2O_3 assumed henceforth.

The filter transmission $T(E)$ is approximated as the product

$$T(E) = \prod_{1}^{n} e^{[-\mu_i(E)\cdot x_i]}, \tag{3}$$

where x_i is the height of the volume occupied by the i'th atomic species and μ_i is its corresponding linear attenuation coefficient. The linear attenuation coefficient is proportional to the imaginary part f_2 of the atomic scattering factors.

On the basis of Eq. (3), we develop a model for filter transmission, directly involving the atomic elements without any further constraint related to the specific material, such as its density and stoichiometry (they shall, however, be considered afterward to estimate each layer thickness).

The model allows for fitting experimental transmission data, provided that the atomic scattering factors are known. For outside absorption edge regions, atomic scattering factors by Henke et al.[28] can be used; however, within edges, we use the model to obtain effective values for f_2 of each element from the data. Specifically, the fit function is based on the product of the transmission due to each element and has four free parameters, the volume depth occupied by each element x_i, as follows:

$$T(E) = T_{Al}T_CT_N\ T_O = e^{[-\mu_{Al}(E)\cdot x_{Al}]}e^{[-\mu_C(E)\cdot x_C]}e^{[-\mu_N(E)\cdot x_N]}e^{[-\mu_O(E)\cdot x_O]}. \tag{4}$$

In Eq. (4), we disregard H since it has a negligible absorption in the energy range of interest.

A preliminary fit was performed outside each element edge region on two reference samples, using Henke tabulated values for f_2. Focusing on one element at a time, e.g., Al, we then modeled the transmission curve within its edge region due to all of the other elements, using the preliminary best-fit parameters x_i. We then divided the experimental transmission (T_{exp}) by the modeled transmission of all of the other elements, given by the product $T_C \cdot T_O \cdot T_N$ in this example. The linear attenuation coefficient (μ_{Al}) can then be calculated by dividing the logarithm of this ratio by the specific element volume height obtained from the preliminary fit. The f_2 inside a specific element edge region is proportional to these values, which are smoothed with a polynomial and interpolated over the energy range, and is derived as in Eq. (5) (example for Al) as

$$(f_2)_{\text{Al}} \propto \mu_{\text{Al}}(E) = \frac{1}{x_{\text{Al}}} \cdot \ln\left(\frac{T_{\text{exp}}}{T_C \cdot T_N \cdot T_O}\right). \tag{5}$$

These effective values for f_2, calculated from the experimental data, are atomic in nature, but they take into account each atom local environment within the material. For instance, since Al is present both in the metallic and aluminum oxide compounds, the f_2 calculated for Al includes both components. This method can be safely applied if edges of different elements do not overlap over the same energy range, as in the case for our samples. Having obtained effective values for f_2 inside each edge, the fit can be performed again, over the whole energy range, now including edge regions. From these best-fit parameters, all layer thicknesses can be estimated, introducing two quantities *a posteriori*: material density and stoichiometry. For instance, PI thickness can be estimated from the best-fit parameter of either C or N. Starting from x_N and dividing it by the product of PI density (1.4 g/cm^3) times the nitrogen mass fraction f_N (PI molecule $C_{22}H_{10}N_2O_4$), PI thickness, $x_{PI(N)}$, is calculated as

$$x_{\mathrm{PI(N)}} = \frac{x_{\mathrm{N}}}{\rho_{\mathrm{PI}} \cdot f_{\mathrm{N}}}, \quad \text{with} \quad f_{\mathrm{N}} = \frac{2A_{\mathrm{N}}}{22A_{\mathrm{C}} + 10A_{\mathrm{H}} + 2A_{\mathrm{N}} + 4A_{\mathrm{O}}}. \tag{6}$$

In principle, the same calculation can be carried out using x_C, but oxygen cannot be used since it is also involved in aluminum oxide. However, knowing the PI layer thickness from N, the Al_2O_3 layer thickness can be derived from the remaining number density of O atoms.

Finally, to define a 3σ confidence interval (CI) and assess the accuracy achievable by the transmission model, the percent relative error (%err) between the best-fit and the data was calculated, and the corresponding CI was estimated by modeling the maximum and minimum fit curves according to the best-fit.

4 Results and Discussion

Experimental transmission data are shown in Fig. 3 for thin samples (X-IFU thermal filters) and in Fig. 4 for thick samples (WFI optical blocking filters), comparing results obtained at different beamlines. It is worth noting that sample part number (PN) 3203 measured at Elettra and PN 3204 measured at SOLEIL come from the same batch, and thus the corresponding transmission data are closer, whereas sample PN 2472 has slightly less Al (see Al L-edge in Fig. 2). The opposite is true for the thick samples, where sample PN 2460 measured at BESSY shows a slightly thicker coating of Al.

In Fig. 5, the fit performed outside edge regions using the tabulated scattering factor is plotted for a reference filter (PN 3096). The experimental data of this filter were used to obtain the effective values for f_2 of elements C, N, and O in the ranges: 280 to 375 eV, 395 to 450 eV,

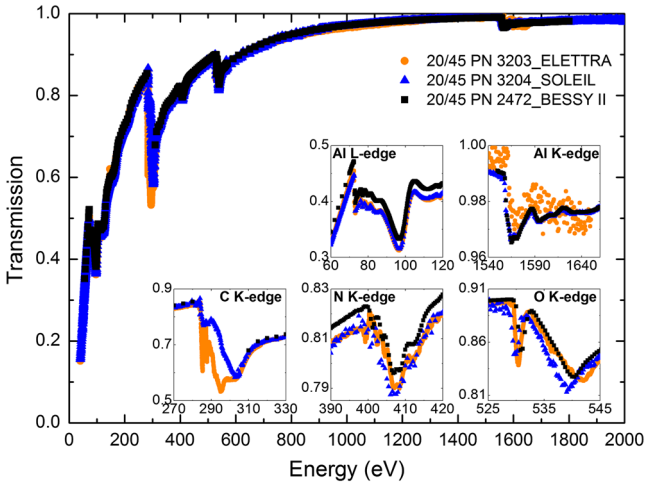

Fig. 3 Comparison between experimental transmission data acquired at Elettra (orange line), SOLEIL (blue line), and BESSY II (black line) on 20/45 thin samples. Data in the C K-edge is absent for BESSY II. Insets show zooms of edges element-wise.

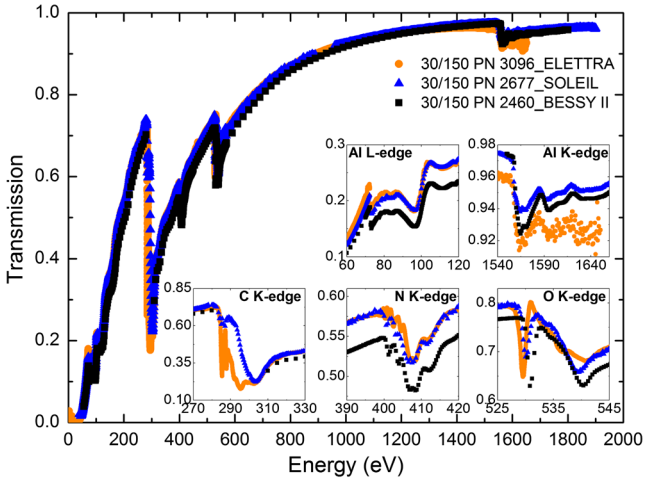

Fig. 4 Comparison between experimental transmission data acquired at Elettra (orange line), SOLEIL (blue line), and BESSY II (black line) on 30/150 thick samples. Data in the C K-edge is absent for BESSY II. Insets show zooms of edges element-wise.

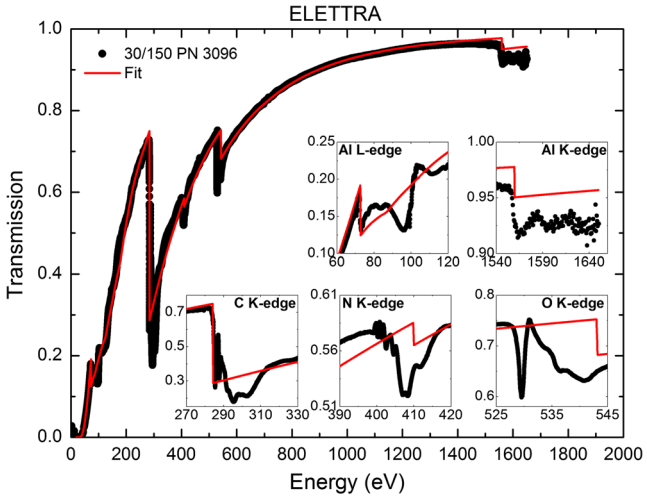

Fig. 5 Experimental data (black dots) of a reference thick sample measured at Elettra (PN 3096), used to obtain effective values of f_2 for C, N, and O after fitting the curve outside edges (red line).

and 527 to 570 eV. A different reference filter (PN 2460) was used to obtain effective values for f_2 of Al inside its L- and K-edges: 72 to 220 eV and 1550 to 1670 eV, respectively.

After obtaining the effective values for f_2 in all of the element edge regions from the reference samples, a best-fit was performed for all of the samples, including edges, to find each layer thickness (see Table 5, where superscript indicates reference samples).

From Table 5, the sum of Al and Al_2O_3 thicknesses is just a few nanometer less than the nominal value provided by the filter manufacturer. This remains true when comparing the equivalent Al amount (equivalent Al in Table 5), calculated from the total number of Al absorbers divided by the Al density 2.7 g/cm^3. Possibly, the actual Al coating density could be slightly lower than expected because of the nanometric scale of the layer and the technological process involved. The Al_2O_3 thickness is in line with what is expected if the spontaneous oxidation process occurred on both surfaces of the Al layer since the value found in the literature is 3 to 4 nm per surface.[29] A slight variability in Al_2O_3 thickness is observed, probably due to different ages of the samples, ranging from a few months to four years old. The thickness of the PI layer estimated from N is in overall good agreement with the nominal thickness, except for the reference sample where it is underestimated. The authors have no clear explanation for

Table 5 Layer thickness of each material (Al, Al_2O_3, and PI) with its 3σ statistical uncertainty in parenthesis, as obtained from the best-fit parameters.

	Best-fit thicknesses (nm)					Nominal thickness (nm)	
Sample (synchrotron)	Al	Al_2O_3	Equivalent Al	PI (from N)	PI (from C)	Al (nm)	PI (nm)
20/45 (Elettra)	9.4 (0.2)	8.5 (0.2)	16.00 (0.02)	45.5 (1.1)	57.8 (0.1)	20.6 (2.5)	45.5 (5)
20/45 (SOLEIL)	9.1 (0.6)	8.5 (0.7)	15.61 (0.06)	49 (4)	58.3 (0.5)	20.6 (2.5)	45.5 (5)
20/45 (BESSY II)	9.3 (1.0)	7.4 (1.1)	15.0 (0.1)	46 (6)	55.9 (1.1)	21.5 (2.5)	42.7 (5)
30/150 (Elettra)[a]	20.6 (0.2)	9.4 (0.3)	27.90 (0.03)	137.5 (1.3)	177.3 (0.2)	31.1 (5)	149.7 (5)
30/150 (SOLEIL)	18.4 (1.5)	11 (2)	26.8 (0.2)	146 (10)	178.0 (1.3)	28.8 (5)	153.4 (5)
30/150 (BESSY II)[a]	23 (3)	10 (4)	30.6 (0.5)	164 (20)	197 (3)	30.4 (5)	157.8 (5)

[a]Reference samples used for the determination of the effective values for f_2 inside edges.

this slight discrepancy; it is possible that using this sample as the reference sample to retrieve the effective f_2 may have influenced the result. In any case, the PI layer thickness from C is consistently overestimated. There are at least two possible explanations: the first one is that samples, which have been exposed to air in some instances, have some C surface contamination; the second is that there is either a different stoichiometry of the PI or carbon-based molecules trapped somewhere within or between layers. We have a few x-ray photoelectron spectroscopy measurements, which preliminarily indicate the presence of C surface contamination.

In Figs. 6–8, datasets of thin samples with their best-fit are shown, whereas a plot with the %err along with its CI is shown in Fig. 9 for a thin sample, with a red vertical line to signal the low energy threshold for the nominal sensitivity of the Athena X-ray sensors (200 eV) and two horizontal lines to display the filter calibration requirement of $\pm 1\%$ relative error.

Data at $E < 200$ eV, where the sample has a lower transmittance, are still important to accurately estimate the Al layer since the L-edge is very sensitive to changes in the number of Al absorbers.

The best-fit is overall in good agreement with all datasets, even inside edge regions. Regarding BESSY II and SOLEIL, the agreement of the fit to the data is very good, with a percent relative error in transmission below 1% everywhere, except in the C, N, and O K-edges, where effective f_2 were obtained from the thick sample measured at Elettra. Looking at the C K-edge measured at SOLEIL, the shape is noticeably different from the same edge measured

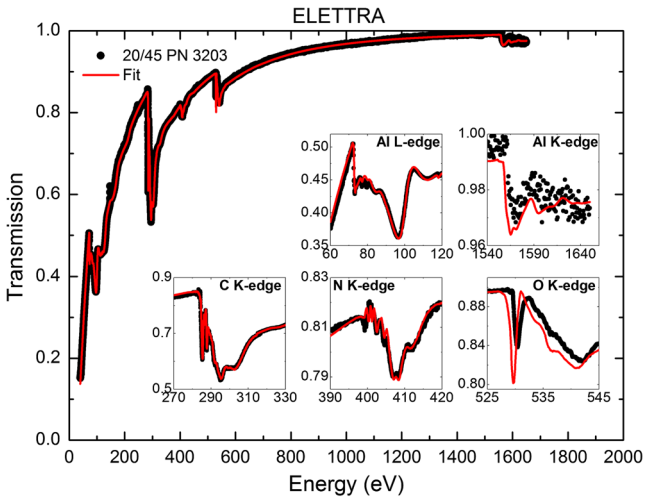

Fig. 6 Dataset of 20/45 sample (black dots) measured at Elettra with its best-fit (red line).

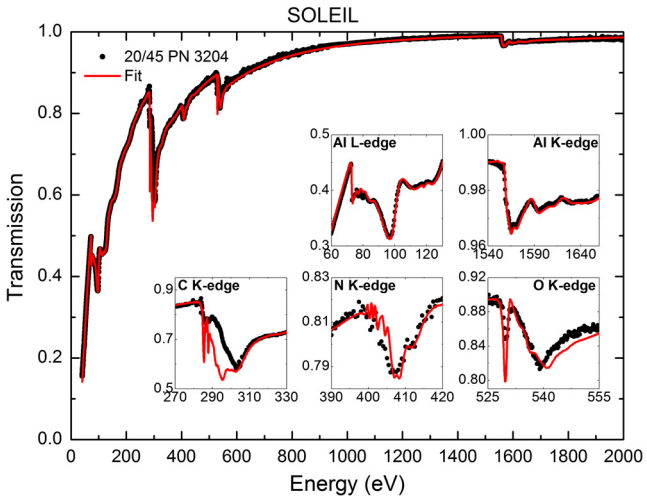

Fig. 7 Dataset of 20/45 sample (black dots) measured at SOLEIL with its best-fit (red line).

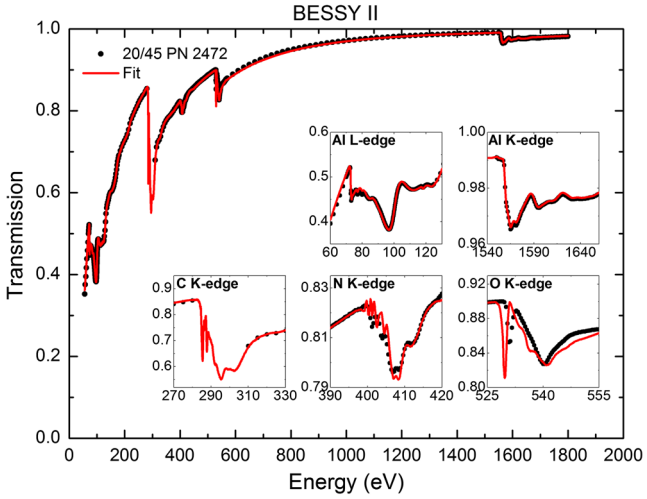

Fig. 8 Dataset of 20/45 sample (black dots) measured at BESSY II with its best-fit (red line).

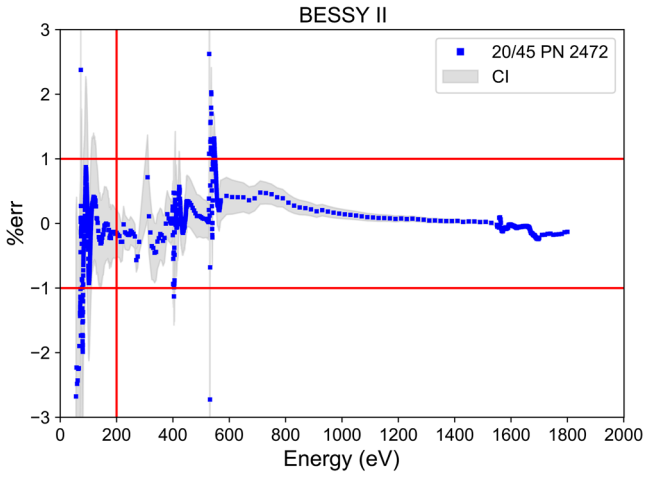

Fig. 9 Percent error (%err) between data and best-fit (blue squares) for sample 20/45 measured at BESSY II with its CI (gray area). Red lines define the range of interest for filter calibration.

Table 6 Percent relative error between data and best-fit for 20/45 samples grouped by energy range (in eV). K-edges are listed separately and the C K-edge is not reported.

Sample (synchrotron)	Percent relative error (%)					
	$0.2 < E < 0.4$ keV	N K-edge	$0.4 < E < 0.6$ keV	O K-edge	$E > 0.6$ keV	Al K-edge
20/45 (Elettra)	$< \pm 1.5$	$< \pm 1$	$< \pm 1$	>3	$< \pm 1$	$< \pm 2.7$
20/45 (BESSY II)	$< \pm 1$	$< \pm 1.2$	$< \pm 1$	>3	$< \pm 1$	$< \pm 1$
20/45 (SOLEIL)	$< \pm 1$	$< \pm 1.7$	$< \pm 1$	>3	$< \pm 1$	$< \pm 1$

at Elettra, making this measurement less reliable (as expected). The N K-edge measured at SOLEIL is also quite noisy, whereas at BESSY the energy step is 1 order of magnitude bigger with respect to that of Elettra. Regarding the O K-edge, the scattering factors were recovered from a thick sample, where the relative amount of O in PI with respect to Al_2O_3 is bigger, also causing a difference in edge shape between thin and thick samples as measured by all beamlines.

Concerning Elettra, the fit is also in good agreement with the data, with a percent relative error in transmission below 1.5% in the energy range of interest for Athena, excluding the C, O, and Al K-edges. Within these edges, the model reproduces the data less well due to the following reasons.

1 A ~0.1-eV shift in the energy calibration of the C K-edge between thin and thick samples. Since the reference sample from which effective f_2 was recovered is the thick one, this shift also reflects on the fit accuracy for the thin sample in this region.
2 BEAR performance at the high-energy end of its range, where it is currently suffering an important contamination of beam purity ascribed to stray zero-order light coming from diffuse scattering at the grating and causing, in data reduction, an unphysical decrease of the transmission as the energy increases. Empirical numerical correction is possible and has been proven of use for spectroscopy purposes, though this fact does not make BEAR the first choice for a quantitative measurement of the transmission in this range.

The agreement between best-fit and the data, in terms of percent relative error, is given in Table 6, grouped by energy range. The N, O, and Al K-edges are reported separately, whereas the more problematic C K-edge is not included.

Overall, the model is in good agreement with the data, in terms of percent relative error. However, some improvement is necessary to meet the X-IFU strict calibration requirements, especially within C and O K-edges, both in terms of obtaining improved effective f_2 and of developing an absolute energy scale calibration strategy. The effective f_2, however, appears well suited to model each element edge region, thus increasing the fit agreement with the data.

5 Conclusions

The two onboard instruments of the astrophysics space mission Athena, X-IFU and WFI, have strict calibration requirements. To meet the goals of the filters calibration plan, we have started several x-ray measurement campaigns, using different European synchrotron radiation facilities. Our aim is to characterize filter materials, presently investigated for the filters preliminary design, and to get some confidence on the measurement accuracies achievable in the flight filters calibration program. More than one facility is needed in this regard, to mitigate the risk of potential unavailability of the beamline during calibration measurements on flight filters.

Transmission data were acquired for six filter samples, made of a thin PI membrane coated with Al, at three different synchrotron facilities: CNR-IOM BEAR at Elettra (Trieste, Italy), PTB-UV at BESSY II (Berlin, Germany), and METROLOGIE at SOLEIL (University of Paris-Saclay, France). A model of the filter transmission as a multi-layer of the elements Al, C, N and O was developed, using each element layer thickness as a free parameter. New effective

values for the imaginary part of the scattering factors were obtained by a preliminary fit of two reference samples, with the goal of refining the fit accuracy within edge regions. The layer thicknesses obtained from the best-fit parameters are, in general, in good agreement with the nominal ones.

The percent relative error between the best-fit and the data was evaluated, to estimate the model accuracy in reproducing the data, in view of satisfying the strict calibration requirements of the X-IFU instrument. A good agreement between the measured transmission and the best-fit was found for all of the sample filters. Finally, actions should be undertaken in acquiring more accurate data, such as developing an absolute energy calibration strategy specific for our samples that takes into account the very strict calibration requirements of X-IFU filters, to be run prior to each experimental campaign, and investigating filter surface C contamination.

Acknowledgments

The use of CNR-IOM BEAR beamline at Elettra was possible through the acceptance of Proposal No. 20170078 titled "XAS of Al/polyimide and Si_3N_4 filters for high-energy resolution detectors in astrophysical missions as ATHENA." The use of PTB-EUV beamline at BESSY II was made available by the ESA within the research project "Large area high-performance optical filters for x-ray instrumentation—LAOF" Contract No. 4000120250/17/NL/BJ. The use of METROLOGIE beamline at SOLEIL was possible through the acceptance of Proposal No. 20180061 titled "ATHENA filters transmission measures." We are grateful to Pascal Mercere and Paulo da Silva for their assistance in using the beamline. This research has received funding from Italian Space Agency (ASI) under Contract Nos. 2015-046-R.0 and 2018-1l.-HH.O and from EU Horizon 2020 Program under the AHEAD project, Grant Agreement No. 654215. We acknowledge fruitful discussions and support by LUXEL corp.

References

1. X. Barcons et al., "Athena: the x-ray observatory to study the hot and energetic Universe," *J. Phys. Conf. Ser.* **610**, 012008 (2015).
2. D. Barret et al., "The ATHENA X-ray Integral Field Unit (X-IFU)," *Proc. SPIE* **10699**, 106991G (2018).
3. S. J. Smith et al., "Transition-edge sensor array development for the ATHENA X-Ray Integral Field Unit," *Proc. SPIE* **10699**, 106991L (2018).
4. N. Meidinger et al., "Development of the Wide Field Imager instrument for ATHENA," *Proc. SPIE* **10699**, 106991F (2018).
5. S. S. Murray et al., "In-flight performance of the Chandra high-resolution camera," *Proc. SPIE* **4012**, 68–80 (2000).
6. G. P. Garmire et al., "Advanced CCD imaging spectrometer (ACIS) instrument on the Chandra X-ray Observatory," *Proc. SPIE* **4851**, 28–44 (2003).
7. M. Weisskopf et al., "Chandra X-ray Observatory overview," *Proc. SPIE* **4012**, 2–16 (2000).
8. T. Takahashi, et al. "Hitomi (ASTRO-H) X-ray Astronomy Satellite," *J. Astron. Telesc. Instrum. Syst.* **4**(2), 021402 (2018).
9. M. E. Eckart et al., "Ground calibration of the Astro-H (Hitomi) soft x-ray spectrometer," *J. Astron. Telesc. Instrum. and Syst.* **4**(2), 021406 (2018).
10. M. Barbera et al., "Baseline design of the thermal blocking filters for the X-IFU detector on board ATHENA," *Proc. SPIE* **9144**, 91445U (2014).
11. M. Barbera et al., "Thermal Filters for the ATHENA X-IFU: ongoing activities toward the conceptual design," *J. Low Temp. Phys.* **184**, 706 (2016).
12. M. Barbera et al., "ATHENA X-IFU thermal filters development status toward the end of the instrument phase-A," *Proc. SPIE* **10699**, 106991R (2018).
13. M. Barbera et al., "ATHENA WFI optical blocking filters development status toward the end of the instrument phase-A," *Proc. SPIE* **10699**, 106991K (2018).
14. P. Peille, "X-IFU performance requirements document," XIFU-RD-SYS-00278-CNES, CNES Technical Report part of the Athena X-IFU I-PRR documentation (2019).

15. X-IFU Instrument Team, "X-IFU thermal filters' stack requirements document," XIFU-RD-10000-00347-CNES, CNES Technical Report part of the Athena X-IFU I-PRR (2019).
16. François Pajot with inputs from the X-IFU Calibration Team, "*X-IFU calibration plan*," XIFU-PL-XCAT-180626-IRAP, IRAP Technical Report part of the Athena X-IFU I-PRR (2019).
17. G. Chartas et al., "ACIS UV/optical blocking filter calibration at the National Synchrotron Light Source," *Proc. SPIE* **2805**, 1–11 (1996).
18. L. K. Townsley et al., "Transmission maps of the ACIS UV/optical blocking filters," *Proc. SPIE* **2805**, 134–145 (1996).
19. R. L. Kelley et al., "The Suzaku high resolution x-ray spectrometer," *Publ. Astron. Soc. Jpn.* **59**(sp1), S77–S112 (2007).
20. http://www.elettra.trieste.it/elettra-beamlines/bear.html.
21. https://www.ptb.de/cms/en/ptb/fachabteilungen/abt7/fb-71/ag-712.html.
22. https://www.synchrotron-soleil.fr/en/beamlines/metrologie.
23. S. Nannarone et al., "The BEAR beamline at Elettra," *AIP Conf. Proc.* **705**, 450 (2004).
24. G. Naletto et al., "A high resolution monochromator covering wide ultraviolet spectral ranges with a single grating," *Pure Appl. Opt.: J. Eur. Opt. Soc. Part A* **1**(6), 347 (1992).
25. F. Scholze et al., "New PTB beamlines for high-accuracy EUV reflectometry at BESSY II," *Proc. SPIE* **4146**, (2000).
26. R. Klein et al., "The electron storage rings MLS and BESSY II as primary radiator normals," *PTB Mitteilungen* **124**(3), 7–15 (2014).
27. M. Idir et al., "Metrology and tests beamline at SOLEIL design and first results," *AIP Conf. Proc.* **1234**, 485 (2010).
28. B. L. Henke et al., "X-ray interactions: photoabsorption, scattering, transmission, and reflection at $E = 50 - 30,000$ eV, $Z = 1 - 92$," *At. Data Nucl. Data Tables* **54**, 181–342 (1993).
29. L. Sciortino et al., "Surface investigation and aluminum oxide estimation on test filters for the ATHENA X-IFU and WFI detectors," *Proc. SPIE* **9905**, 990566 (2016).
30. M. Barbera et al., "Effects of interference and oxidation on the UV/visible rejection properties of filters for soft X-ray detectors," *Exp. Astron.* **7**, 51–63 (1997).
31. M. Barbera et al., "Status of the EPIC thin and medium filters on-board XMM-Newton after more than 10 years of operation I: laboratory measurements on back-up filters," *Proc. SPIE* **8859**, 885914 (2013).

Elena Puccio received her master's degree in physics and obtained her PhD in physics in 2017 working on big data, network theory, correlation, and cluster analysis. She is currently a postdoc researcher at the University of Palermo, Italy, with a three-year fellowship, affiliated with Istituto Nazionale di AstroFisica–Osservatorio Astronomico di Palermo (INAF-OAPa), to work on the design, development, experimental characterization, and modeling of optical blocking filters and thermal filters for the WFI and X-IFU instruments on board the large astrophysics mission Athena funded by the ESA.

Michela Todaro is a physicist and obtained her PhD in material science and nanotechnology in 2018. She won a postdoc scholarship at the Astrophysics National Institute (INAF-OAPA) in 2018 on remote sensing through aerostatic devices. Currently, she has a postdoctoral fellowship at the University of Palermoon the experimental characterization of the spectral and morphological properties of prototype filters of the X-IFU and WFI instruments on board the ATHENA mission of the ESA.

Ugo Lo Cicero received his PhD in electronic engineering, and is a senior technologist at INAF. He works on the development of new technologies for astrophysics, in particular related to x-ray instrumentation. He has worked on the design and development of microcalorimeter arrays, active optics, and x-ray sources and on the design and extensive characterization of cryogenic x-ray filters. He is system manager for the "thermal filters" subsystem of the X-IFU instrument on board the ESA flagship mission Athena.

Luisa Sciortino received her PhD in chemistry in 2012. She has been working on the development and design of the thermal and optical blocking filters of the X-IFU and WFI instruments on

board the Athena mission. Her expertise is the spectroscopic characterization of materials and nanomaterials. She is currently a researcher in the Department of Physics and Chemistry at the Università degli Studi di Palermo.

Philippe Laurent is working at the Centre for Extragalactic Astronomy (CEA) Astrophysical Department in France. He specialized in high-energy astrophysics and obtained his PhD in 1992, studying black holes x-ray binaries high-energy emission. In parallel, he developed a theoretical model of radiation transfer in the environment of black holes. He has participated in the ESA/INTEGRAL gamma-ray mission since 1995 and is now the Imager on Board the INTEGRAL Satellite (IBIS) telescope Co-PI. He is also co-chair of the ATHENA background studies topical group.

Philippe Ferrando obtained his PhD in high-energy astrophysics in 1987. He has been working on, and was Co-PI of, cosmic-rays instruments on board HEAO3, Voyager, and Ulysses. In 1995, he focused on x-rays and was responsible for the calibration team of the EPIC cameras on XMM-Newton. He has been the principal investigator of several mission proposals and phase-A studies, in particular, the SIMBOL-X hard x-rays telescope. He is currently the deputy head of the CEA Astrophysics Department.

Angelo Giglia obtained his degree in engineering of telecommunications in 1999 and his PhD in 2006 in engineering of materials and environment. He has been a technologist and beamline scientist for experiments for absorption X, reflectivity, and photoemission spectroscopies at the synchrotron beamline at Elettra of the CNR-IOM Laboratory since April 2002 with a permanent position. His activity consists mainly in the use of UV-soft x-rays synchrotron light for the characterization of materials and devices.

Stefano Nannarone graduated in physics from the University Roma La Sapienza in 1967. Presently, he is retired from the University of Modena-Reggio Emilia (professor of general physics), is an associated fellow of CNR, and is the scientist responsible of IOM-CNR synchrotron beamline BEAR (Elettra, Italy). His scientific activity covered electronic and structural properties of solids, surfaces, and interfaces studied by optical (lab and synchrotron) and electron scattering techniques. His teaching experience included general and solid-state physics, solid-state devices, and elementary quantum chemistry.

Marco Barbera obtained his PhD in physics. He works as an associate professor of astrophysics at the University of Palermo, Italy (2004). He is affiliated with INAF-OAPa with responsibilities in the operation of x-ray astronomy calibration and testing facility for development/test of instrumentation for x-ray astronomy missions (filters, optics, and detectors) such as Chandra, Newton-XMM, Hinode, Chang'E-1, Coronas Photons, Athena, and eXTP. He is responsible for the development of filters for the WFI and X-IFU instruments on board the ESA space mission Athena.